Published November , 1982

ATP Reactivation of the Rotary Axostyle in Termite Flagellates: Effects of Dynein ATPase Inhibitors

MICHAEL A. YAMIN and SIDNEY L. TAMM

Boston University Marine Program, Marine Biological Laboratory, Woods Hole, Massachusetts 02543. Dr. Yamin's present address is Evreka Inc., Bergenfield, New Jersey 07621

ABSTRACT The anterior end or head of a devescovinid flagellate from termites continually rotates in a clockwise direction relative to the rest of the cell. Previous laser microbeam experiments showed that rotational motility is caused by a noncontractile axostyle complex which runs from the head through the cell body and generates torque along its length.

We report here success in obtaining glycerinated cell models of the rotary axostyle which, upon addition of ATP, undergo reactivation and exhibit rotational movements similar to those observed in vivo. Reactivation of rotational motility and flagellar beating of the models requires ATP or ADP and is competitively inhibited by nonhydrolyzable ATP analogs (AMP-PNP and ATP-γ-S). *N*-ethylmaleimide, *p*-hydroxymercuribenzoate, and mersalyl acid also blocked reactivation of both the rotary axostyle and flagella. Vanadate and erythro-9-[3-(2-hydroxynonyl)]-adenine (EHNA) selectively inhibited flagellar reactivation without effecting rotational motility. These results, together with previous ultrastructural findings, suggest that the rotary axostyle does not operate by a dynein-based mechanism but may be driven by an actomyosin system with a circular arrangement of interacting elements.

Most types of nonmuscle cell motility involve contractile, translational, or bending movements and are thought to operate by an ATP-powered sliding filament (or microtubule) mechanism as in muscle (13, 22, 32, 44).

Recently, however, other mechanisms of motility not based on actomyosin or tubulin-dynein mechanochemistry have been reported. These exceptional types of motility include the contraction of spasmonemes and myonemes in ciliate protozoa (2, 7, 17), rowing beats of the axopods of the heliozoan *Sticholonche zanclea* (7, 8), active bending of the costa of trichomonad flagellates (1), contraction of flagellar rootlet fibers in algae (34), and rotation of bacterial flagella (3, 4, 36). In the last case, the existence of a rotary motor inside cells was demonstrated for the first time; furthermore, the bacterial flagellar motor is unusual in that it does not use ATP directly but is driven by a protonmotive force (21, 25, 26).

We recently discovered another example where nature has invented the wheel—but in a eukaryotic cell (37–39, 42, 43). One part of a devescovinid flagellate from termites continually rotates in the same direction relative to the rest of the cell. Rotational motility is caused by a rodlike axostyle complex which runs from the anterior to the posterior end of the cell and generates torque along its length (38).

A major question is whether the axostylar rotary motor works by a cross-bridge driven shearing interaction between some of its components or whether it is another exception to this scheme. As pointed out for bacterial motility, "the existence of a rotary motor ... need not involve any novel biological principles" (23). "There is no fundamental conceptual difference between the mutual sliding of elements in a linear fashion (as in muscle or eukaryotic cilia) and sliding in a closed circle (as in bacterial flagella)" (24).

Indeed, the ultrastructure and geometry of the axostyle complex suggests that it may generate torque by a conventional actomyosin sliding mechanism, but with a novel arrangement of the interacting parts. The axostyle itself is a rod of longitudinally oriented microtubules. Encircling the microtubular bundle is a single-layered sheath of microfilaments that run at right angles to the microtubules and therefore parallel to the direction of rotation and presumed force production. The microfilament sheath is surrounded by a differentiated girdle of cytoplasm consisting of an inner layer of fibrillar material and membranous elements and an outer region of membrane-bounded granules. We previously suggested that if the microfilaments contain actin and are firmly anchored to the microtubular rod, they might interact with a hypothetical myosin framework in the surrounding girdle to produce sliding forces which would turn the axostyle (37, 38).

Published November , 1982

Here we report a significant advance for testing this idea and analyzing how the rotary axostyle works. We have obtained semi-permeabilized cell models of the axostylar rotary motor which reactivate upon addition of ATP and exhibit rotational motility similar to that observed in vivo. This allows the chemical and ionic requirements of the motile apparatus to be determined and the effects of specific mechanochemical inhibitors to be tested dynamically. Our results suggest that the rotary axostyle may indeed operate by a conventional actomyosin sliding mechanism, but with a new twist.

MATERIALS AND METHODS

Organism

The protozoan is the same devescovinid flagellate from *Cryptotermes cavifrons* used in previous studies (37–43). This flagellate has not yet been named but closely resembles *Caduceia kofoidi* described by Kirby (18). Wood containing *C. cavifrons* was collected in southern Florida and stored in the laboratory until used for obtaining termites.

Reagents

ATP and norepinephrine were obtained from Calbiochem-Behring Corp., San Diego, CA; erythro-9-[3-(2-hydroxynonyl)]adenine (EHNA) from Burroughs Wellcome, Detroit, MI; adenosine-5′-0-(3-thiotriphosphate) (ATP-γ-S) from Boehringer-Mannheim Biochemicals, Indianapolis, IN; adenylyl-imidodiphosphate (AMP-PNP), *N*-ethyl maleimide (NEM), fluorescein isothiocyanate-conjugated dextrans (FITC-dextran), fluorescein diacetate, mersalyl acid, and *p*-hydroxymercuribenzoate (PCMB) from Sigma Chemical Co., St. Louis, MO; sodium vanadate from Mallinckrodt Inc., St. Louis, MO. Calcium buffers containing EGTA were prepared according to Salmon and Segall (35).

Extraction and Reactivation

Hindguts from 2–3 termites were placed in 50 μl of extraction solution (ES) in a depression plate. All steps were done at room temperature. ES consisted of 15% glycerol, 12.5 mM PIPES, pH 6.9. The guts were teased open to release the protozoa, and the tissue was discarded. After 3 min, extracted cells were diluted into reactivation solution (RS). The proportion of solutions mixed was always one part of cells in ES: one part 3× RS: one part deionized water or 3× test solution. Standard 3× RS contained 30 mM PIPES, 7.5 mM ATP, 7.5 mM $MgCl_2$, 15 mM EGTA, and 150 mM KCl, pH 6.9, so that final concentrations during reactivation were 14 mM PIPES, 2.5 mM ATP, 2.5 mM $MgCl_2$, 5 mM EGTA, 50 mM KCl, and 5% glycerol. Control RS lacked ATP. For observations of reactivation, 10 μl of cells in ES, 10 μl of 3× RS, and 10 μl of water or 3× test solution were thoroughly mixed together on a microscope slide, covered with a 22-mm^2 coverslip, and examined with a Zeiss Universal microscope. To observe the extraction process itself, a hindgut was opened directly into 30 μl of ES on a microscope slide, and the morphology of the cells was followed during the 3-min extraction period.

Light Microscopy of Reactivation

The patterns and extent of reactivation were observed by Zeiss phase-contrast or Nomarski optics. Rates of rotation of various cell parts or organelles were measured with a stopwatch. To test the effects of compounds on reactivation (Table I), the extent of reactivation in a given preparation was estimated as follows. For rotational motility, the percent of models showing head rotation (the most common pattern) was scored in more than 100 cells on the slide. A rating of +++ indicated that >50% of the models were undergoing head rotation; ratings of ++, +, and ± represent 25–50%, 2–25%, and <2% of the models exhibiting head rotation, respectively. A rating of − indicated no observed rotation (0%). Similarly, a partially subjective determination of the vigorousness of flagellar beating was made in reactivated models, with a rating of +++ indicating activity similar to that in vivo in virtually all the models, and a rating of − representing complete absence of any flagellar beating.

The morphology and patterns of rotational motility of reactivated models were recorded on Kodak Technical Pan (2415) film using a Zeiss Ukatron electronic flash. Cine films of reactivated models were taken with a Locam 16-mm camera (Redlake Lab, Santa Clara, CA) on Kodak Plus-X Negative film at 12 or 25 fps.

Permeability of Models

Living flagellates were labeled internally with fluorescein before extraction by incubating cells in 50 mM PIPES, pH 6.9, containing 1 μg/ml fluorescein diacetate for 3 min under a stream of humid N_2. After this time, flagellates remained active and became intensely fluorescent due to intracellular accumulation of fluorescein (33). Cells were then diluted into excess ES, and release of fluorescein was observed with Zeiss epifluorescence optics.

The ability of dyes and fluorescein-conjugated macromolecules to penetrate cells during extraction or reactivation was determined by including the dyes or labeled molecules in the ES or RS and observing under brightfield or fluorescence optics for entry of the compound into the cells.

Electron Microscopy of Reactivated Models

Extracted models were placed in RS or in RS containing 10 μM vanadate for 3 min, sampled for determination of the percentage of cells undergoing head rotation, and immediately fixed in 2% paraformaldehyde, 1.5% glutaraldehyde, 0.1 M sodium phosphate buffer (pH 7.0) for ~1 h. Approximately 55% of the models showed head rotation at the time of fixation in both reactivation solutions, but flagellar beating was inhibited in RS containing vanadate (see below).

Living control cells were placed in 0.6% NaCl for 3 min before fixation. About 85% of the cells had rotating heads at this time.

After glutaraldehyde fixation, all batches were washed in buffer, postfixed in 2% OsO_4, 0.1 M phosphate buffer for 1 h, washed in water, and stained in 0.5% uranyl acetate for 2 h. Dehydration in acetone was followed by gradual infiltration in Araldite. Sections were cut with a diamond knife, placed on formvar-coated grids, stained with uranyl acetate and lead citrate, and examined in a Philips 300 or Zeiss 10CA electron microscope at 80 kV.

RESULTS

Structure and Rotational Motility of Living Devescovinids

The ultrastructure and remarkable rotational motility of this protozoan have been described previously (37–43). A brief summary is presented here for comparison with reactivated cell models.

Devescovinids are 100–150 μm long and zeppelin-shaped when freshly removed from termites. Three anterior flagella and a longer recurrent flagellum arise from the caplike anterior end or head of the cell.

The head of the devescovinid continually rotates in a clockwise direction (as viewed anteriorly) relative to the cell body, which either may turn in the opposite direction or remain stationary. Laser microbeam experiments showed that rotational movements are caused by a rodlike axostyle complex that runs from the head to the posterior end of the cell and generates torque along its length (38). The rotary axostyle does not actively bend or undulate as do the contractile axostyles of other insect flagellates (5, 15, 20, 27, 29, 46).

The axostyle itself is a cochleate spiral of ~400 microtubules running parallel to the rod axis (Fig. 1). At the anterior end the axostylar microtubules enclose the nucleus and continue under the surface of the head (Fig. 2). The helical Golgi apparatus is wrapped tightly around the anterior trunk of the axostyle (Fig. 2), and the flagellar basal bodies and rootlets are also attached to the axostylar microtubules. The axostyle-flagella-nucleus-Golgi complex rotates as a unit, thereby coupling axostyle rotation with head rotation.

Just posterior to the Golgi apparatus is a cup-shaped group of endosymbiotic bacteria through which the axostyle passes (Figs. 2 and 3). This bacterial cup has never been observed to rotate independently around the axostyle in living cells.

The microtubular rod of the axostyle is surrounded along most of its length by a single-layered sheath of microfilaments. The microfilaments run at right angles to the microtubules and appear as rings encircling the microtubular spiral in transverse

Published November , 1982

sections through the axostyle (38) (Fig. 1). Surrounding this sheath is a differentiated girdle of cytoplasm which appears by light microscopy as a narrow clear inner zone (inner girdle) and a more irregular outer layer of granules and refractile particles (outer girdle). In thin sections, the inner girdle consists of fine fibrillar material with interspersed membranous elements, and the outer girdle contains membrane-bound dense bodies resembling hydrogenosomes (30) (Fig. 1). Rotation of the outer girdle around the axostyle normally accompanies counterclockwise rotation of the cell body.

Extraction Process and General Features of Cell Models

Freshly isolated devescovinids were used for making cell models. The conversion of living cells into models was followed by phase-contrast microscopy during the 3-min extraction period. Freshly released flagellates placed in ES immediately become shriveled and condensed, resembling crenated bananas, and rotational movements stop. Flagellar activity continues but ceases within 1–2 min. The cell then begins to swell and bleb at multiple locations. Many fine particles are released into the medium at discrete sites around the perimeter of the cell and gradually drift away. Granules present within the swollen parts of the cell show Brownian movement. Swollen regions tend to coalesce with one another, and wood chips often remain localized in a dense mass in one part of the cell.

The cell membrane remains smooth and rounded as swelling occurs. The ectosymbiotic bacteria lose their ordered arrangement and become irregularly distributed over the cell surface. The head of the models usually remains distinct, but in some cells with swollen anterior ends the head becomes incorporated into the main cell body ("headless", Fig. 3, *b*, *g*, *h*, *k*, *l*). The axostyle complex appears preserved intact, although granules of the outer girdle may be missing in certain regions.

Reactivation of Motility in Cell Models

When extracted cells are placed in RS, the flagella begin to beat and various types of rotational movements appear. In RS without ATP, no flagellar reactivation or rotational motility occurs (Table I). Flagellar beating and rotational motility may be started in such preparations, however, by perfusion of RS containing ATP under the coverslip. The different patterns of rotational movements observed in reactivated cell models are described below.

CLOCKWISE ROTATION OF AXOSTYLE-FLAGELLA-GOLGI-NUCLEUS COMPLEX (HEAD): In models with distinct heads, the head rotates continually in a clockwise direction as in living cells, while the body usually does not turn. The asymmetrical papillar side of the head with its emergent flagella serves as a convenient marker for following head rotation (Fig. 3 *c–f*). If the axostyle is bowed, it wobbles with a periodicity the same as that of head rotation, showing that it indeed rotates (Fig. 3 *e–j*). Neither the bacterial cup nor the granules surrounding the axostyle rotate in most models. Unlike the situation in living cells, the shear zone between the head and body is usually constricted to the width of the axostyle and is located between the Golgi apparatus and the bacterial cup (Figs. 3 *e* and *f*, and 2). The anterior rim of the bacterial cup appears closely apposed to the cell membrane, just posterior to the shear zone (Fig. 2). The pronounced constriction of the shear zone in cell models results from head rotation; nonreactivated models in RS without ATP rarely show such constrictions.

TABLE I

Effects of Nucleotides and Inhibitors on Reactivation of Flagellar vs. Rotational Motility

Compound*	Flagellar activity	Rotational motility
0 mM ATP	–	–
0.1 mM ATP	±	–
0.5–5.0 mM ATP	+++	+++
2.5 mM ADP	+++	+++
3.3 mM GTP	+	–
4.0 mM AMP-PNP	–	–
4.0 mM AMP-PNP + 1 mM ATP	–	±
3.3 mM ATP-γ-S	–	–
3.3 mM ATP-γ-S + 0.5 mM ATP	–	–
3.3 mM ATP-γ-S + 2.5 mM ATP	+	++
1.0 mM Mersalyl acid or PCMB + 2.5 mM ATP	–	–
3.3 mM NEM + 2.5 mM ATP	–	–
4.0 mM EHNA + 1.0 mM ATP	–	++
10 μM Vanadate + 2.5 mM ATP	–	+++
100 μM Vanadate + 2.5 mM ATP	–	++
500 μM Vanadate + 2.5 mM ATP	–	±
10 μM Vanadate + 2.5 mM ATP + 2.5 mM norepinephrine	+++	+++

See Materials and Methods for explanation of plus/minus ratings.
* In RS without ATP unless indicated.

In most RS preparations, >50% of the models undergo reactivation of head rotation and flagellar beating. Some cells show flagellar reactivation without head rotation and, less commonly, reactivation of head rotation in the absence of flagellar activity. The velocity of head rotation in RS (2.5 mM ATP) ranges from <0.03 rotation/s to 0.25 rotation/s, with rates of 0.07–0.2 rotation/s being most common. The maximum speed of head rotation observed in reactivated models is thus close to that observed in freshly isolated living cells. Rotational velocities of cell models are maintained for 15–20 min in slide preparations and then gradually decline, though some rotation can still be seen after 1–2 h in slide preparations sealed with vaseline.

In some ballooned or flattened models where a distinct head is absent, the axostyle-nucleus-Golgi complex still rotates, pushing the flagella around through the cell membrane at the anterior end (Fig. 3 *g* and *h*). The bacterial cup and outer girdle granules are usually stationary, except as noted below.

COUNTERCLOCKWISE ROTATION OF THE CELL BODY: When head rotation of reactivated models is obstructed, the cell body rotates in a counterclockwise direction, as observed in living cells with tethered heads (42). Occasionally, models exhibit both clockwise rotation of the head and counterclockwise rotation of the body, as typically found in freshly released living flagellates (39, 42).

COUNTERCLOCKWISE ROTATION OF THE BACTERIAL CUP: In some models, particularly those without distinct heads, the bacterial cup alone rotates counterclockwise around the anterior end of the axostyle. In such cells the bacterial cup appears free and not connected by its anterior edge to the cell membrane. The rotation velocity of the cup is difficult to determine because of its radial symmetry, but maximum speeds were estimated at 0.2–0.3 rotation/s. Independent rotation of the bacterial cup has never been observed in living cells (38).

COUNTERCLOCKWISE REVOLUTION OF GRANULES AROUND THE AXOSTYLE: Under certain conditions of reactivation, neither the head nor the cell body rotates, but granules of the outer girdle revolve around the axostyle in a

Published November , 1982

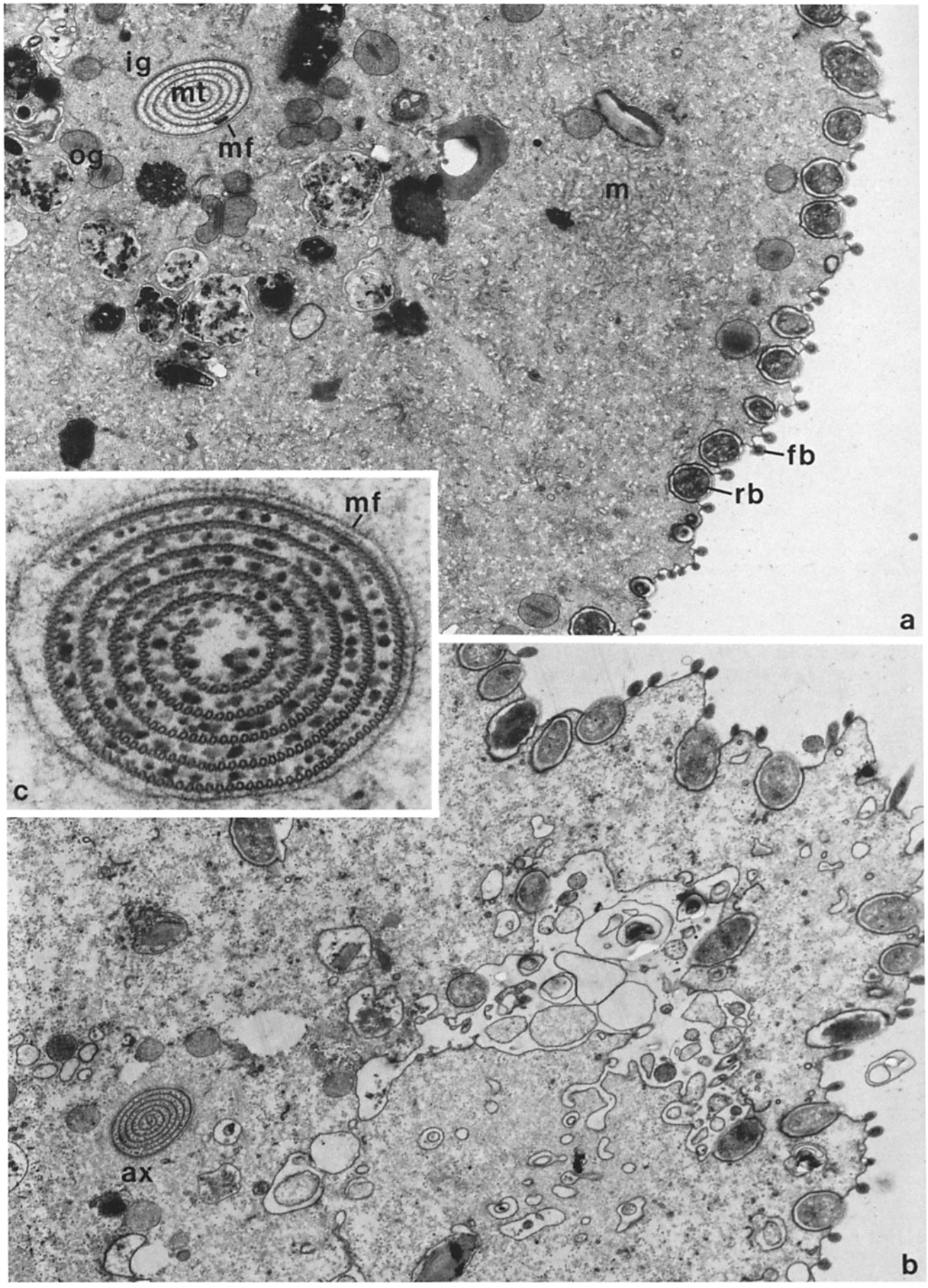

Published November , 1982

counterclockwise direction (Fig. 3 *b*, *k*, and *l*). This pattern is prevalent after 15–30 min on slides, when models, which initially showed clockwise rotation of the head in fresh preparations, become flattened by the coverslip as the preparation dries down. Rotation of granules around the axostyle may also be induced by mechanical disruption of the models, by passage of models through a syringe needle before reactivation, or by tapping on the coverslip.

The entire outer girdle, segments thereof, or even individual granules may revolve around the axostyle. The speed of granule revolution is constant along the length of the axostyle, with maximal rates of 0.2–0.3 rotation/s. Rotation of the outer girdle may be accompanied by rotation of the bacterial cup, particularly if granules adjacent to the cup are revolving around the axostyle (Fig. 3 *b*). In such models, the bacterial cup and outer girdle turn as a unit at the same speed.

Counterclockwise revolution of granules around a nonrotating axostyle, so-called "reactive torque", also occurs in living cells, particularly after treatment with polyene antibiotics (38).

DISPLACED SHEAR ZONE: In certain cases, the shear zone is shifted posterior to its normal location, so that the head includes the nucleus, Golgi apparatus, and, in addition, the bacterial cup and some body cytoplasm (Fig. 3 *i* and *j*). This enlarged head rotates clockwise as a unit, at speeds up to 0.25 rotation/s. The shear zone of such models is always constricted to the width of the axostyle, sometimes with only a short length of axostyle connecting the two parts of the model. Displaced and constricted shear zones have also been observed occasionally in living cells under unfavorable conditions (42).

OTHER PATTERNS OF ROTATIONAL MOTILITY IN REACTIVATED MODELS: Different permutations of the above patterns of rotation were observed occasionally. In some "headless" models, clockwise rotation of the axostyle-Golgi-nucleus complex alternated with counterclockwise rotation of the bacterial cup and outer girdle granules around the axostyle. In one case, the bacterial cup became separated from the head and cell body by membrane constrictions on either side and rotated counterclockwise between the stationary head and body.

Requirements for Reactivation

Inclusion of ATP or ADP in RS was essential for reactivation of both flagellar beating and rotational motility. The ability to use ADP indicates that adenylate kinase activity is present in the cell models. Non-hydrolyzable ATP analogs, AMP-PNP and ATP-γ-S, failed to support flagellar or axostylar reactivation. When present in excess over ATP concentration, these compounds competitively inhibited motility (Table I). GTP supported only flagellar reactivation, but at a low beat frequency.

The threshold concentration of ATP for reactivation of rotation was 0.25 mM, but rotation velocities were slow at this concentration. Normal (maximal) speeds were observed over a range of 0.5–5 mM ATP, with rotation velocity decreasing at higher ATP concentrations (Table I). The threshold ATP concentration for flagellar reactivation was 0.1 mM (Table I). Mg^{+2} was required for flagellar and axostyle reactivation.

Reactivation of rotational motility occurred over a pH range of 6.5–8.0, with optimal activity at pH 6.9–7.5. Free calcium concentrations from 10^{-8} to 5×10^{-4} had no obvious effect on either direction or speed of rotation, though at the high end of the range the rotation speed was slightly lower.

Effects of ATPase Inhibitors on Motility

SULFHYDRYL POISONS: Mersalyl acid, PCMB, and NEM block free sulfhydryl groups, thereby inhibiting dynein and myosin ATPase activity. 1 mM mersalyl or PCMB in RS inhibited reactivation of both flagellar and rotational motility (Table I). 3.3 mM NEM immediately stopped flagellar activity and caused a reduction in the speed of head rotation for ~10 s before rotation completely stopped. During this time, the head of the rotating models appeared to extrude slightly from the cell, leaving only a short length of axostyle connecting the two parts of the cell. Including 5 mM DTT with NEM prevented inhibition of flagellar and rotational motility.

VANADATE: Vanadate in the +5 oxidation state is a potent inhibitor at micromolar levels of dynein ATPase activity and reactivated beat of cilia and flagella but does not affect myosin ATPase or glycerinated myofibril contraction except at millimolar concentrations, and then only slowly (10–12, 14, 19, 45).

Inclusion of 5 μM vanadate in RS inhibited reactivation of the anterior flagella and most recurrent flagella but had no effect on rotational motility. 10 μM vanadate suppressed all flagellar activity, yet rotational movements continued normally (Table I). As the concentration of vanadate in RS was increased above 100 μM, rotation speeds decreased, but even at 500 μM vanadate some models were observed with very slowly rotating heads. Addition of 2.5 mM norepinephrine reversed the inhibition of flagellar beating by low concentrations of vanadate, presumably by reducing the metal to the inactive +4 oxidation state (18, 28). Flagellar activity and rotational movements of living cells were not affected by millimolar concentrations of vanadate in saline medium.

EHNA: EHNA is a weaker but more selective inhibitor of dynein ATPase activity and flagellar beating, with no effect or even a stimulatory action on myosin ATPase activity (6, 9, 31). When present at excess over ATP concentrations, EHNA blocked reactivation of flagellar beating in the models but allowed rotational motility to continue (Table I).

FIGURE 1 Electron micrographs of living devescovinid (*a*) and reactivated cell models (*b*, *c*). (*a*) Transverse thin section through flagellate fixed in vivo in 0.6% NaCl. The axostyle complex consists of a spiral sheet of microtubules (*mt*), microfilament sheath (*mf*), inner cytoplasmic girdle (*ig*), and outer girdle of dense granules (*og*) (see text). The cytoplasm contains numerous membranous elements (*m*) distributed throughout a dense ground substance. Ectosymbiotic rod (*rb*) and fusiform (*fb*) bacteria, here cut transversely, are attached to the surface by specific junctional complexes (40). (*b*, *c*) Transverse sections through reactivated cell models fixed in RS + 10 μM vanadate (see Materials and Methods). Axostyle rotation but not flagellar beating is reactivated. The structure of the axostyle complex (*ax*) is preserved, including the microfilamentous sheath encircling the microtubular coil (*mf* in *c*). However, the cytoplasm appears extracted and the fine membranous inclusions present in living cells (*a*) are missing. Instead, large irregular vesicles are invaginated from the plasma membrane. The cell membrane itself appears intact, without obvious holes or discontinuities. Sections are viewed from the anterior end of the cell. *a* and *b*, × 12,000. *c*, × 69,000.

Published November , 1982

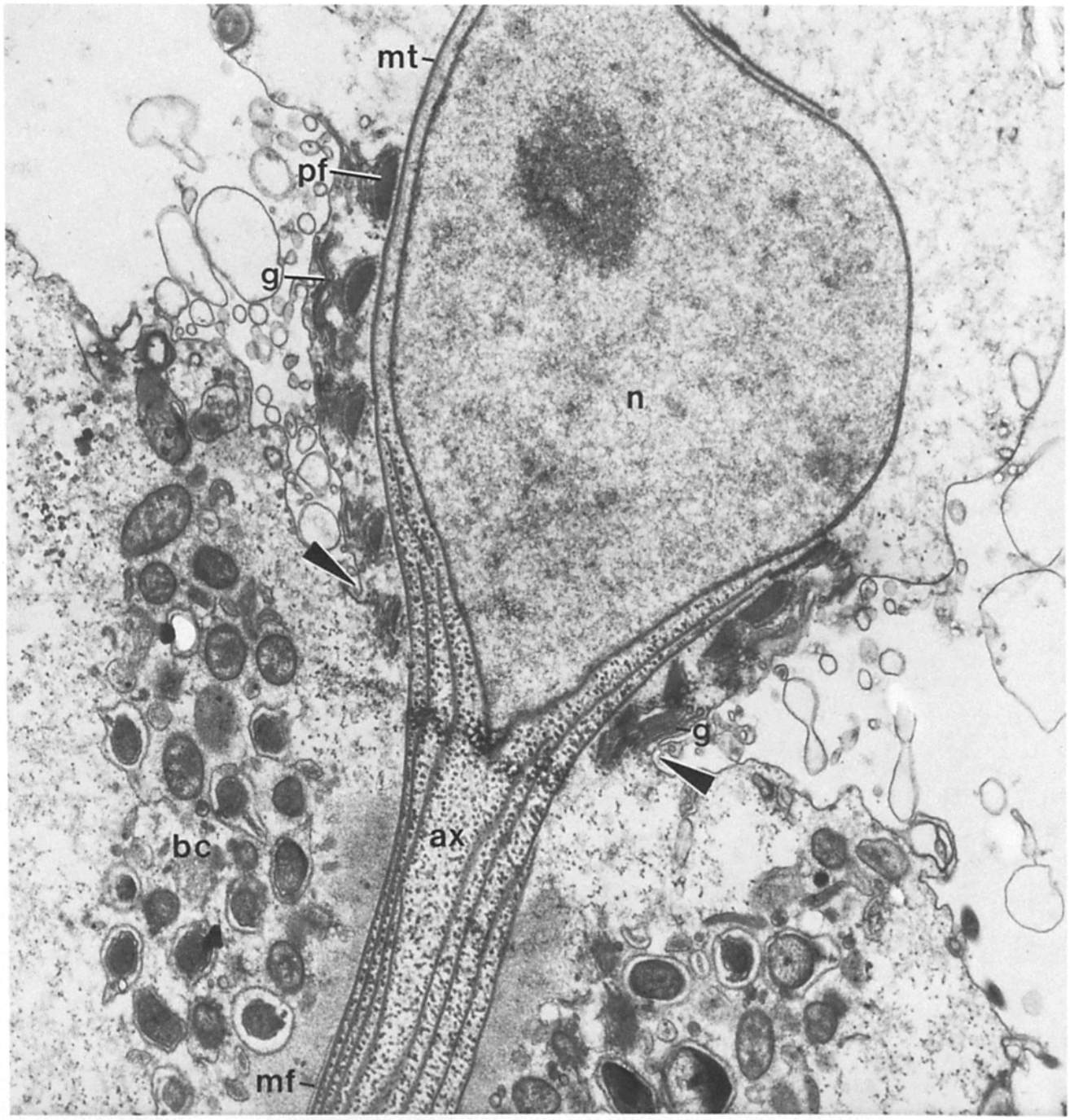

FIGURE 2 Longitudinal thin section through the anterior end of a reactivated cell model fixed in RS + 10 μM vanadate. Head rotation has caused the shear zone (arrowheads) to become constricted to the width of the axostyle (*ax*) between the posteriormost coil of the Golgi apparatus (*g*) and the anterior rim of the cup-shaped group of endosymbiotic bacteria (*bc*) (see Fig. 3 *e*, *f*). Note numerous vesicles and membrane protrusions in the vicinity of the shear zone. Axostyle microtubules (*mt*) run alongside the nucleus (*n*) and continue into the head. Coils of the helical Golgi apparatus and underlying parabasal filament (*pf*), here cut transversely, are wrapped around the nucleus and trunk of the axostyle. Note that the anterior rim of the bacterial cup is closely applied to the surface of the broadened "shoulders" of the cell body. The termination of the microfilamentous sheath (*mf*) surrounding the axostyle microtubules is evident within the bacterial cup. × 18,000. For comparison to in vivo structure, see reference 42, Fig. 3, and reference 38, Fig. 2.

Permeability of Cell Models

Living flagellates, prelabeled with fluorescein, rapidly lost fluorescence when placed in ES. The release of intracellular fluorescein (mol wt, 332) indicates a rapid increase in membrane permeability to small molecules after ES treatment.

The dyes erythrosin B (mol wt, 880) and patent blue V (mol wt, 1,159) did not enter living cells in saline but entered extracted models. Two FITC-dextrans, molecular weights 17,500 and 67,600, failed to enter either living cells or cell models, as did FITC-goat anti-rabbit immunoglobulin. These macromolecules were unable to enter models during extraction, or during subsequent reactivation. Under fluorescence optics the cells and models appeared as black silhouettes against a

Published November , 1982

bright green background. However, if various detergents were included in the ES or RS, or added to ES or RS, cell models became permeable to these labels, but rotational motility stopped (even in the absence of the FITC-dextrans). This effect occurred at very narrow detergent thresholds, e.g., between 0.04% and 0.05% Nonidet P-40. Detergents also caused the cell membrane to appear jagged and rough, in contrast to the smooth rounded appearance of membranes in standard ES containing glycerol.

Ultrastructure of Cell Models

The ultrastructure of cell models fixed in RS or in RS + 10 μM vanadate is identical and is similar to that of living cells in several respects (Figs. 1 and 2). Most cell models have an intact axostyle complex, including the microtubular spiral, microfilamentous sheath, and surrounding cytoplasmic girdle (Fig. 1). The plasma membrane of models also appears intact: no holes or visible disruptions in unit membrane morphology were detected. This evident integrity of the plasma membrane in electron micrographs conceals the permeability of models to small molecules (see above) but accurately reflects their impermeability to larger molecules.

Ectosymbiotic bacteria are irregularly distributed on the surface of models, in contrast to their orderly arrangement on living cells (40). In addition, membrane blebs and whorls are often associated with the surface of cell models, but not living cells. This is particularly evident at the constricted shear zone between the head and body of many models (Fig. 2).

The cytoplasm, which in living cells contains numerous granules and membranous elements, appears mostly devoid of these inclusions in cell models (Fig. 1). The cytoplasm of extracted cells is noticeably less dense and more homogeneous in appearance compared with living cells and often contains large vesicles derived from the plasma membrane (Fig. 1 *b*).

DISCUSSION

We report here success in obtaining glycerinated cell models of a rotary axostyle which, upon addition of ATP, undergo reactivation and exhibit rotational movements similar to those observed in living flagellates. The ability to experimentally manipulate the chemical and ionic environment of the torque-generating machinery enables the mechanism underlying this remarkable motility to be analyzed by dynamic, functional criteria. In addition, the flagella of the models provide an internal control for comparing the axostylar rotary motor to dynein-based motile systems.

The various patterns of rotational motility obtained in reactivated models indicate that relative torque is generated between the axostyle and the surrounding cytoplasmic girdle, confirming previous laser microbeam experiments on living devescovinids (38). Most models behaved like living cells, in which active rotation of the axostyle within the cell body turns organelles (nucleus, Golgi apparatus, flagella) connected to its anterior end, thereby causing clockwise rotation of the head. In other models, where cytoplasmic connections anchoring the bacterial cup and granules of the outer girdle are presumably broken, either or both of these structures revolve counterclockwise around the axostyle. Such examples of reactive torque have been seen in living cells, with the exception of rotation of the bacterial cup (38). In most models, the bacterial cup appears connected to the plasma membrane just posterior to the shear zone and does not rotate. However, in cases where the bacterial cup is separated from the membrane (i.e., in "headless" models), it often does turn. Since the microfilamentous sheath of the axostyle extends partially into the bacterial cup (38) (Fig. 2), some rotation of this structure might be expected (see below).

With regard to energy requirements, the rotary axostyle is similar to actomyosin and tubulin-dynein based motile systems, in that ATP hydrolysis is necessary for chemomechanical transduction. The eukaryotic rotary motor is fundamentally different in this respect from the rotary motor driving bacterial flagella, which uses protonmotive force, not ATP directly, as the energy source (21, 25, 26). The axostylar rotary motor is also unlike the spasmoneme-myoneme system of ciliates, where Ca^{++} alone triggers coiling of 20 Å filaments, without any direct involvement of ATP (2).

The insensitivity of rotational motility to vanadate and EHNA clearly distinguishes the rotary axostyle from the cell's flagella and indicates that a dynein-like ATPase is not involved in the rotary motor. However, this conclusion remains tentative, because the flagella may not be a valid control for comparing effects of dynein ATPase inhibitors on the rotary motor. Because the axostyle is located inside the cell body, it may be less accessible to vanadate and EHNA than are the flagella. This possibility seems unlikely, however, since molecules larger than these inhibitors, i.e., ATP, can readily enter the models and reach the axostyle. In addition, EHNA freely penetrates living cells (6).

Another possible reason for the insensitivity of rotational motility to vanadate and EHNA, besides lack of involvement of dynein ATPase, is the fundamentally different structure and type of motility of the axostyle complex compared to flagella. For example, the axostylar motor may operate by a dynein-based mechanism but be more efficient than flagella, i.e., the number of dynein-catalyzed interactions required to produce rotation may be considerably less than that necessary to generate bends in flagellar axonemes. Rotational motility would then appear relatively insensitive to vanadate and EHNA, yet the motor could still involve dynein. Finally, a potential axostyle "dynein" might not contain vanadate or EHNA-sensitive sites and thus may be different from the flagellar dynein of the devescovinid.

Nevertheless, the present findings are consistent with our previous suggestion, based entirely on ultrastructural evidence, that the rotary axostyle operates by an actomyosin rather than a tubule-dynein mechanism (37, 38). The filaments surrounding the microtubular coil are similar in size to actin filaments and run in the direction of rotation, i.e., parallel to the expected direction of force generation. If the microfilaments contain actin and are firmly attached to the microtubule rod, they could be actively sheared by a myosin framework in the surrounding girdle, thereby causing unidirectional rotation of the axostyle.

Thus, the unusual rotational motility of the devescovinid may be generated by a conventional actomyosin sliding filament mechanism, but with a circular arrangement of interacting elements. A remarkably similar type of mechanism drives the rotation of actin filament rings isolated from *Nitella* endoplasm (16).

Because the reactivated models described here are not permeable to large molecules, we have not been able to test specific inhibitors of actin-myosin vs. tubulin-dynein interactions, such as NEM-modified HMM or S_1 (28), or antibodies against these contractile proteins. However, the finding that

Published November , 1982

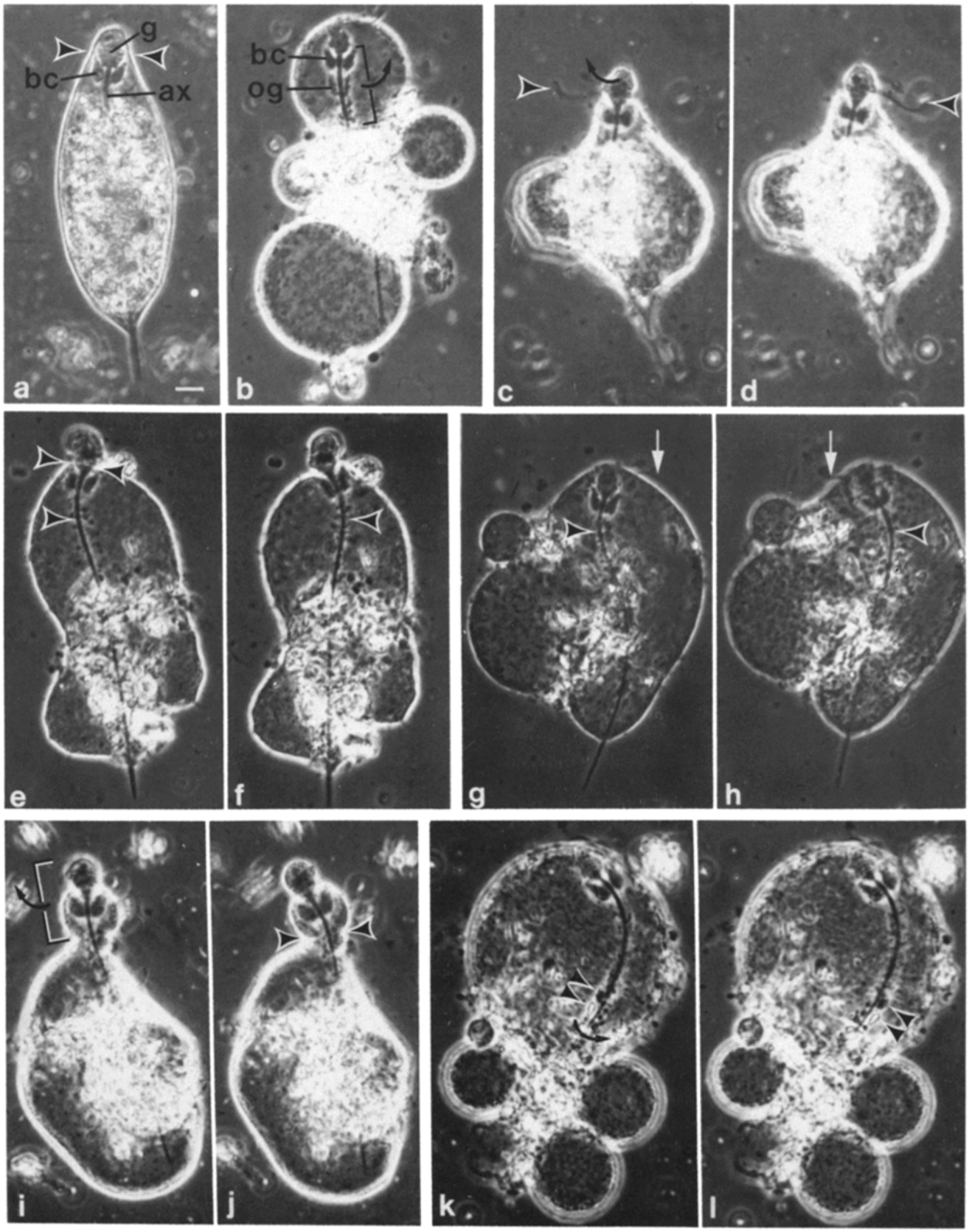

rotation continues in reactivated models which are torn open offers an approach for using these probes to analyze the molecular basis of the rotary motor.

We thank Signhild Tamm for help in electron microscopy, and Robert Syren for collecting termites in Florida.

This work was supported by National Institutes of Health grant GM-27903.

Received for publication 17 May 1982, and in revised form 9 August 1982.

REFERENCES

1. Amos, W. B., A. V. Grimstone, L. J. Rothschild, and R. D. Allen. 1979. Structure, protein composition, and birefringence of the costa: a motile flagellar root fiber in the flagellate *Trichomonas*. *J. Cell Sci.* 35:139–164.
2. Amos, W. B., L. M. Routledge, T. Weis-Fogh, and F. F. Yew. 1976. The spasmoneme and calcium-dependent contraction in connection with specific calcium-binding proteins. *In* Calcium in Biological Systems. C. J. Duncan, editor. *Symp. Soc. Exp. Biol.* Cambridge Univ. Press. 30:273–301.
3. Berg, H. C., and R. A. Anderson. 1973. Bacteria swim by rotating their flagellar filaments. *Nature (Lond.)*. 245:380–382.
4. Berg, H. C. 1974. Dynamic properties of bacterial flagellar motors. *Nature (Lond.)*. 249:77–79.
5. Bloodgood, R. A. 1975. Biochemical analysis of axostyle motility. *Cytobios*. 14:101–120.
6. Bouchard, P., S. M. Penningroth, A. Cheung, C. Gagnon, and C. W. Bardin. 1981. *erythro*-9[3-(2-Hydroxynonyl)] adenine is an inhibitor of sperm motility that blocks dynein ATPase and protein carboxylmethylase activities. *Proc. Natl. Acad. Sci. U. S. A.* 78:1033–1036.
7. Cachon, J., and M. Cachon. 1981. Movement by non-actin filament mechanisms. *Biosystems*. 14:313–326.
8. Cachon, J., M. Cachon, L. G. Tilney, and M. Tilney. 1977. Movement generated by interactions between the dense material at the ends of microtubules and non-actin-containing microfilaments in *Sticholonche zanclea*. *J. Cell Biol.* 72:314–338.
9. Cande, W. Z. 1982. Inhibition of spindle elongation in permeabilized mitotic cells by erythro-9-[3-(2-hydroxynonyl)] adenine. *Nature (Lond.)*. 295:700–701.
10. Cande, W. Z., and S. M. Wolniak. 1978. Chromosome movement in lysed mitotic cells is inhibited by vanadate. *J. Cell Biol.* 79:573–580.
11. Cantley, L. C., L. Josephson, R. Warner, M. Yanagisawa, C. Lechene, and G. Guidotti. 1977. Vanadate is a potent (Na, K)-ATPase inhibitor found in ATP derived from muscle. *J. Biol. Chem.* 252:7421–7423.
12. Gibbons, I. R., M. P. Cosson, J. A. Evans, B. H. Gibbons, B. Houck, K. H. Martinson, W. S. Sale, and W.-J. Y. Tang. 1978. Potenti inhibition of dynein adenosine triphosphatase and of the motility of cilia and sperm flagella by vanadate. *Proc. Natl. Acad. Sci. U. S. A.* 75:2220–2224.
13. Goldman, R., T. Pollard, and J. Rosenbaum. 1976. Cell Motility. *Cold Spring Harbor Conf. Cell Prolif.* 3:1–1373.
14. Goodno, C. C. 1979. Inhibition of myosin ATPase by vanadate ion. *Proc. Natl. Acad. Sci. U. S. A.* 76:2620–2624.
15. Grimstone, A. V., and L. R. Cleveland. 1965. The fine structure and function of the contractile axostyle of certain flagellates. *J. Cell Biol.* 24:387–400.
16. Higashi-Fujime, S. 1980. Active movement in vitro of bundles of microfilaments isolated from *Nitella* cell. *J. Cell Biol.* 87:569–578.
17. Huang, B., and D. Mazia. 1975. Microtubules and filaments in ciliate contractility. *In* Molecules and Cell Movement. S. Inoué and R. E. Stephens, editors. Raven Press, NY. 389–409.
18. Kirby, H. 1949. Devescovinid flagellates of termites. V. The genus *Hyperdevescovina*, the genus *Bullanympha*, and undescribed or unrecorded species. *Univ. Calif. Publ. Zool.* 45:319–422.
19. Kobayashi, T., T. Martensen, J. Nath, and M. Flavin. 1978. Inhibition of dynein ATPase by vanadate, and its possible use as a probe for the role of dynein in cytoplasmic motility. *Biochem. Biophys. Res. Commun.* 81:1313–1318.
20. Langford, G. M., and S. Inoué. 1979. Motility of the microtubular axostyle in *Pyrsonympha*. *J. Cell Biol.* 80:521–538.
21. Larsen, S. H., J. Adler, J. J. Gargus, and R. W. Hogg. 1974. Chemomechanical coupling without ATP: the source of energy for motility and chemotaxis in bacteria. *Proc. Natl. Acad. Sci. U. S. A.* 71:1239–1243.
22. Lazarides, E., and J. P. Revel. 1979. The molecular basis of cell movement. *Sci. Am.* 240:100–113.
23. Macnab, R. M. 1978. Bacterial motility and chemotaxis: the molecular biology of a behavioral system. *Crit. Rev. Biochem.* 5:291–341.
24. Macnab, R. M. 1980. Sensing the environment. Bacterial chemotaxis. *In* Biological Regulation and Development, Vol. 2. R. F. Goldberger, editor. Plenum Press, NY. 377–412.
25. Manson, M. D., P. Tedesco, H. C. Berg, F. M. Harold, and C. van der Drift. 1977. A protonmotive force drives bacterial flagella. *Proc. Natl. Acad. Sci. U. S. A.* 74:3060–3064.
26. Matsuura, S., J. Shioi, and Y. Imae. 1977. Motility in *Bacillus subtilis* driven by an artificial protonmotive force. *FEBS (Fed. Eur. Biochem. Soc.) Lett.* 82:187–190.
27. McIntosh, J. R., E. S. Ogata, and S. C. Landis. 1973. The axostyle of *Saccinobaculus*. *J. Cell Biol.* 56:304–323.
28. Meeusen, R. L., and W. Z. Cande. 1979. *N*-ethylmaleimide-modified heavy meromyosin. A probe for actomyosin interactions. *J. Cell Biol.* 82:57–65.
29. Mooseker, M. S., and L. G. Tilney. 1973. Isolation and reactivation of the axostyle. Evidence for a dynein-like ATPase in the axostyle. *J. Cell Biol.* 56:13–26.
30. Muller, M. 1980. The hydrogenosome. *In* The Eukaryotic Microbial Cell. G. W. Gooday, D. Lloyg, and A. P. J. Trinci, editors. *Soc. Gen. Microbiol. Symp.* Cambridge Univ. Press, England. 30:127–142.
31. Penningroth, S. M., A. Cheung, P. Bouchard, C. Gagnon, and C. W. Bardin. 1982. Dynein ATPase is inhibited selectively in vitro by erythro-9-[3-2-(hydroxynonyl)]adenine. *Biochem. Biophys. Res. Commun.* 104:234–240.
32. Pollard, T. D., and R. R. Weihing. 1974. Actin and myosin and cell movement. *CRC Crit. Rev. Biochem.* 2:1–65.
33. Rotman, B., and B. W. Papermaster. 1966. Membrane properties of living mammalian cells as studied by enzymatic hydrolysis of fluorogenic esters. *Proc. Natl. Acad. Sci. U. S. A.* 55:134–141.
34. Salisbury, J. L., and G. L. Floyd. 1978. Calcium-induced contraction of the rhizoplast of a quadriflagellate green alga. *Science (Wash. D. C.)*. 202:975–977.
35. Salmon, E. D., and R. R. Segall. 1980. Calcium-labile mitotic spindles isolated from sea urchin eggs (*Lytechinus variegatus*). *J. Cell Biol.* 86:355–365.
36. Silverman, M., and M. Simon. 1974. Flagellar rotation and the mechanism of bacterial motility. *Nature (Lond.)*. 249:73–74.
37. Tamm, S. L. 1976. Properties of a rotary motor in eukaryotic cells. *In* Cell Motility. R. Goldman, T. Pollard, and J. Rosenbaum, editors. Cold Spring Harbor Conferences on Cell Proliferation, vol. 3. Cold Spring Harbor Laboratory, NY. 949–967.
38. Tamm, S. L. 1978. Laser microbeam study of a rotary motor in termite flagellates. Evidence that the axostyle complex generates torque. *J. Cell Biol.* 78:76–92.
39. Tamm, S. L. 1979. Membrane movements and fluidity during rotational motility of a termite flagellate. *J. Cell Biol.* 80:141–149.
40. Tamm, S. L. 1980. The ultrastructure of prokaryotic-eukaryotic cell junctions. *J. Cell Sci.* 44:335–352.
41. Tamm, S. L. 1982. Flagellated ectosymbiotic bacteria propel a eukaryotic cell. *J. Cell Biol.* 94:697–709.
42. Tamm, S. L., and S. Tamm. 1974. Direct evidence for fluid membranes. *Proc. Natl. Acad. Sci. U. S. A.* 71:4589–4593.
43. Tamm, S. L., and S. Tamm. 1976. Rotary movements and fluid membranes in termite flagellates. *J. Cell Sci.* 20:619–639.
44. Taylor, D. L., and J. S. Condeelis. 1979. Cytoplasmic structure and contractility in amoeboid cells. *Int. Rev. Cytol.* 56:57–144.
45. Wolniak, S. M., and W. Z. Cande. 1980. Physiological requirements for ciliary reactivation of bracken fern spermatozoids. *J. Cell Sci.* 43:195–207.
46. Woodrum, D. T., and R. W. Linck. 1980. Structural basis of motility in the microtubular axostyle: implications for cytoplasmic microtubule structure and function. *J. Cell Biol.* 87:404–414.

FIGURE 3 Phase contrast micrographs showing rotational motility of reactivated cell models in RS (*b–l*). (*a*) Unextracted flagellate freshly removed from termite gut and fixed in OsO_4 vapor. Appearance is identical to that of the living cell. Note bacterial cup (*bc*), helical Golgi apparatus (*g*), and axostyle (*ax*). Paired arrowheads indicate the location of the shear zone between head and body. Refractile wood chips fill much of the body cytoplasm. (*b*) Reactivated "headless" cell model in which the bacterial cup (*bc*) and segment of the outer girdle (*og*) revolve around the axostyle in a counterclockwise direction (bracket and arrow). Although the cell is swollen in several different regions, the plasma membrane appears smooth and rounded; wood chips are concentrated in the mid-region of the model. (*c–l*) Pairs of micrographs showing rotating structures of reactivated models at two extreme positions differing by 180°. (*c*, *d*) Reactivated model undergoing clockwise rotation of the head (arrow); recurrent flagellum appears on opposite sides as the head turns (arrowheads). (*e*, *f*) Clockwise rotation of bowed axostyle (arrowheads) and head. The shear zone (paired arrowheads in *e*) is constricted to the width of the axostyle between the Golgi apparatus and the bacterial cup. Electron micrograph through this region in another model is shown in Fig. 2. (*g*, *h*) Reactivated "headless" model in which the bowed axostyle (arrowheads), Golgi apparatus, and nucleus are rotating as a unit in a clockwise direction. The flagella (arrows) are pushed around through the plasma membrane at the anterior end. (*i*, *j*) Model in which the shear zone (paired arrowheads in *j*) is displaced posterior to the bacterial cup; the head, bacterial cup, and additional cytoplasm rotate clockwise (bracket, arrow in *i*). (*k*, *l*) "Headless" model in which the axostyle does not rotate, but particles surrounding the axostyle revolve around it in a counterclockwise direction (arrow). Particles appearing on left side of the axostyle in *k* have rotated 180° to the right side of the axostyle in *l* (arrowheads). Bar, 10 μm. × 500.